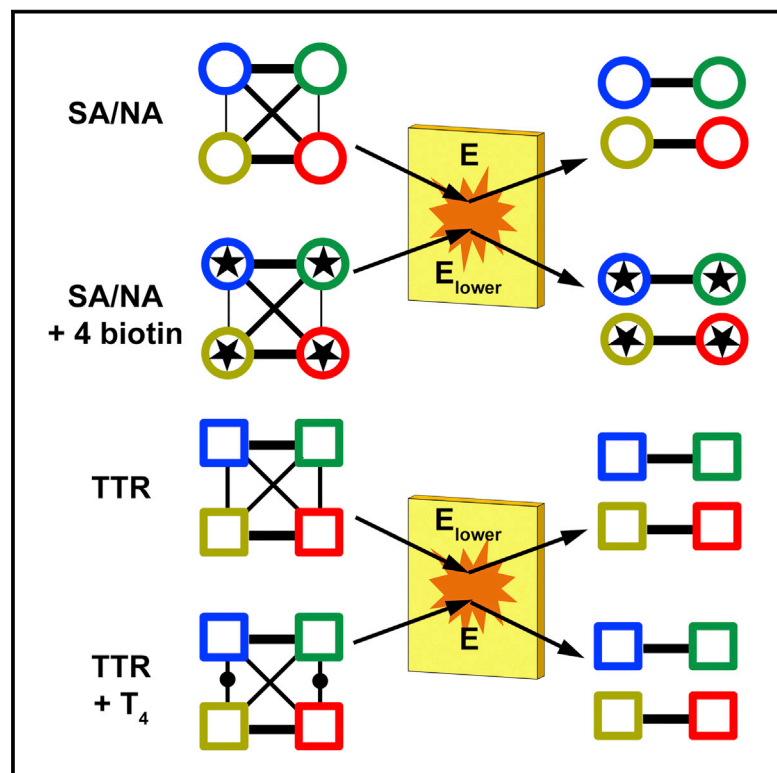


# Chemistry & Biology

## Surface-Induced Dissociation of Homotetramers with $D_2$ Symmetry Yields their Assembly Pathways and Characterizes the Effect of Ligand Binding

### Graphical Abstract



### Authors

Royston S. Quintyn, Jing Yan, Vicki H. Wysocki

### Correspondence

wysocki.11@osu.edu

### In Brief

Gas-phase dissociation pathways observed for homotetramers upon collision with a surface depend on the interface area and thus give insight into their solution-phase assembly pathways. Quintyn et al. apply the approach to protein complexes with ligands bound and confirm that changes in conformational flexibility and tetramer stability depend on ligand binding location.

### Highlights

- Surface collision of  $D_2$  tetramers yields dimers that further fragment to monomers
- Collision energy needed for dissociation tracks with dimer-dimer interface area
- Location of ligand binding sites affects tetramer dissociation behavior



# Surface-Induced Dissociation of Homotetramers with $D_2$ Symmetry Yields their Assembly Pathways and Characterizes the Effect of Ligand Binding

Royston S. Quintyn,<sup>1,2</sup> Jing Yan,<sup>1,2</sup> and Vicki H. Wysocki<sup>1,\*</sup>

<sup>1</sup>Department of Chemistry and Biochemistry, Ohio State University, Columbus, OH 43210, USA

<sup>2</sup>Co-first author

\*Correspondence: [wysocki.11@osu.edu](mailto:wysocki.11@osu.edu)

<http://dx.doi.org/10.1016/j.chembiol.2015.03.019>

## SUMMARY

Understanding of protein complex assembly and the effect of ligand binding on their native topologies is integral to discerning how alterations in their architecture can affect function. Probing the disassembly pathway may offer insight into the mechanisms through which various subunits self-assemble into complexes. Here, a gas-phase dissociation method, surface-induced dissociation (SID) coupled with ion mobility (IM), was utilized to determine whether disassembly pathways are consistent with the assembly of three homotetramers and to probe the effects of ligand binding on conformational flexibility and tetramer stability. The results indicate that the smaller interface in the complex is initially cleaved upon dissociation, conserving the larger interface, and suggest that assembly of a  $D_2$  homotetramer from its constituent monomers occurs via a  $C_2$  dimer intermediate. In addition, we demonstrate that ligand-mediated changes in tetramer SID dissociation behavior are dependent on where and how the ligand binds.

## INTRODUCTION

The majority of proteins exist *in vivo* as oligomers with varying quaternary structural attributes, rather than as individual chains (Shen and Chou, 2009). Approximately 50%–70% of oligomers with known quaternary structure are homomers, which are formed by the assembly of identical protein subunits (Goodsell and Olson, 2000; Levy et al., 2006). These homomers often adopt highly symmetrical structures, with most having either cyclic ( $C_n$ ) or dihedral ( $D_n$ ) symmetry (Levy et al., 2008). Homomerization and the evolutionary selection of symmetry is driven by functional, genetic, and physicochemical needs (Goodsell and Olson, 2000). For example, self-assembly of the p53 tumor suppressor protein into a homotetramer with  $D_2$  symmetry enables it to bind variably spaced DNA target sequences, essential for p53 transactivation and tumor suppressor functions (Okorokov et al., 2006). The misfolding and subsequent misassembly of homomers into structures that deviate from their native functional

conformational state is a major contributing factor in a wide array of human diseases (Kelly, 1997; Ng et al., 2012; Wetzel, 1996). Consequently, developing an understanding of how different subunits interact to form functional protein complexes is key to gaining insight into how these homomers carry out their normal biological functions and how alterations in their architecture lead to malfunction.

In recent years, native mass spectrometry (MS) coupled with ion mobility (IM) has emerged as a powerful tool for probing the assembly of protein complexes, as it is capable of simultaneously identifying the various subcomplexes produced after solution disruption of subunit interfaces within oligomers (Hernandez and Robinson, 2007; Levy et al., 2008). The perturbation of subunit interfaces can occur in solution by changing the ionic strength (Kapur et al., 2002; Kershaw et al., 2002), pH (Light-Wahl et al., 1994), or adding organic solvents (Gupta et al., 2004).

The dissociation of oligomers can also occur in the gas phase; collision-induced dissociation (CID) is the most popular method available in commercial mass spectrometers. In CID, however, the precursor ion undergoes multiple low-energy collisions with an inert low-mass gas, which typically produces fragmentation patterns that are not representative of the oligomer substructure (an unfolded monomer and  $(n - 1)$  multimer), and thus provides limited information on the assembly of these oligomers (Benesch et al., 2006). Alternatively, there is substantial evidence illustrating that fragmentation is more reflective of multimer architecture in surface-induced dissociation (SID) (Blackwell et al., 2011; Zhou and Wysocki, 2014), where ions undergo a collision with a surface target often composed of a fluorinated alkanethiol self-assembled monolayer (Jones et al., 2006). SID is a fast, high-energy deposition process (Blackwell et al., 2011), and thus allows for better characterization of the oligomer assembly, because faster structurally informative dissociation pathways can outcompete the slower monomer unfolding (rearrangement) dissociation pathway observed in CID (Zhou et al., 2013). Although previous studies utilizing solution disruption followed by MS detection demonstrated that the assembly/evolutionary pathway of an oligomer is the reverse of the dissociation process (Levy et al., 2008), the utilization of SID as a direct means of discerning the assembly pathway of oligomers has not been systematically investigated.

A statistical distribution of the various types of quaternary structures that existed in the Swiss-Prot databank in April, 2008, revealed that the majority of oligomers exist either as dimers or tetramers (Shen and Chou, 2009). Moreover, dihedral

homomers are over ten times more abundant than cyclic homomers with the same numbers of subunits (Levy et al., 2008). A search of the PDB reveals that the majority of homomers with crystal structures are either dimers or have dihedral symmetry (Marsh and Teichmann, 2014). Because our research focuses on self-assembly, we chose homotetramers with  $D_2$  symmetry as model systems for our study. In the present study, we utilize three  $D_2$  homotetramers (transthyretin, streptavidin, and neutravidin, the deglycosylated form of avidin) as model systems. We determine whether the assembly pathway inferred from SID dissociation (disassembly) is similar to that previously described for  $D_2$  tetramers where monomers  $\rightarrow$   $C_2$  dimers  $\rightarrow$   $D_2$  tetramer (Villar et al., 2009).

One of the many functional benefits associated with the self-assembly of monomers into oligomers is that it can occasionally facilitate the formation of active sites and ligand binding sites at homomeric interfaces (Marsh and Teichmann, 2014). This is the case for transthyretin (TTR), whose function as a thyroid hormone ( $T_4$ ,  $T_3$ ) transporter is dependent on the assembly into the tetramer, because the ligand binding sites are located at the dimer-dimer interface (Nencetti and Orlandini, 2012). The main biological function of both streptavidin and avidin is as an antibiotic, through mediation by their interaction with biotin (Green, 1990; Weber et al., 1989). While only a single residue (Trp 120 in streptavidin and Trp 110 in avidin) from one monomer makes contact with biotin bound in an adjacent monomer through the dimer-dimer interface in the streptavidin tetramer, previous studies demonstrate that mutation of this residue results in a significant decrease in biotin affinity (Sano and Cantor, 1995).

The presence of low-stability regions within a protein complex appears to provide a mechanism for eliciting high ligand binding affinity (Luque et al., 2002), with binding often triggering changes in protein structure and conformational flexibility that correlate to changes in thermal stability (Celej et al., 2003). By using CID coupled with IM-MS, Hyung et al. (2009) demonstrated that monitoring the unfolding and dissociation of the TTR tetramer allows for the investigation of the stability differences between wild-type and disease-associated variants of TTR not normally observed by MS alone. Studies conducted in the Wysocki laboratory have demonstrated that protein subunits produced by SID of ligand bound complexes such as tryptophan synthase (Quintyn et al., 2013) and C-reactive protein (our unpublished data) retain their ligands, indicating retention of protein fold or at least retention of the ligand binding pocket. Hence, the second part of this research focuses on the application of SID to characterize the changes in stability and conformational flexibility induced by binding of  $T_4$  (TTR) and biotin (streptavidin and neutravidin).

## RESULTS

### Predicting Assembly Pathways of Homotetramers with $D_2$ Symmetry by Surface-Induced Dissociation

Previous studies reported in the literature showed that the largest interfaces are formed first during homomer assembly, and thus the assembly of homomers can be predicted by using a model in which the interface strength is assumed to be proportional to the interface area calculated from crystal structures (Chen et al., 2013; Levy et al., 2008). Considering that SID yields

fragmentation more reflective of multimer architecture, we were interested in determining whether this interface model could be applied to the SID dissociation of the  $D_2$  homotetramers. To test this model, we first calculated the interface areas from the crystal structures of three homotetramers, streptavidin, neutravidin, and TTR (Figures 1A, 1D, and 1G), using PISA analysis (Krisinel and Henrick, 2007). As shown in Table 1, SID of the three tetramers can conceivably yield primary noncovalent cleavage of different interfaces to produce a variety of products, with dimer formation favored over other products.

The SID dissociation of the charge-reduced +11 streptavidin tetramer at 330 eV (Figure 1B) yields primarily dimer. However, it is apparent from Table 1 that there are three possible types of dimers that can be produced from the cleavage of different interfaces by SID. Based on the large differences in the total interface area cleaved, cleavage to form I-IV and II-III dimers is expected. Using the drift times obtained from IM, it was determined that the experimental collision cross section (CCS) of the observed dimer is consistent with the calculated CCS of the dimer expected from cleavage of the lowest total interface area ( $1176 \text{ \AA}^2$ ), assuming no collapse before IM measurement (Figure 2A). Once we established that low-energy SID results in cleavage of a dimer-dimer interface, we subsequently employed higher SID collision energies to determine whether we could observe fragments that represent cleavage of larger total interface area. The increase in the intensity of the monomers at higher SID collision energies (Figure 1B, 770 eV and 1650 eV) may suggest subsequent secondary cleavage of the monomer-monomer interface ( $1551 \text{ \AA}^2$ ) within the initially formed dimer. However, the presence of monomer and trimer fragments at the onset for monomer fragmentation also suggests cleavage of all three interface types to yield monomer and its complementary trimer (requiring cleavage of a total interface area of  $2139 \text{ \AA}^2$ ). The fact that this pathway is observed after dimer-dimer cleavage is consistent with cleavage of the lowest total interface area ( $1176 \text{ \AA}^2$ ) first to form dimer at lower energy followed by cleavage of the next lowest total interface area ( $2139 \text{ \AA}^2$ ). In addition, another alternative pathway may be the direct dissociation of tetramer to four monomers but that would require cleavage of four interfaces with a total interface area of  $4278 \text{ \AA}^2$ . Using IM, it is possible to deduce the relative intensities of the different subunits present at each collision energy, e.g. the IM-MS plot shown in Figure S1A illustrates that the relative abundance of each individual subunit present can be determined by summing the intensities of highlighted regions separately. Therefore, to resolve the pathways responsible for the increase in the monomer intensity at higher energies, we plotted the relative abundance of the various subunits produced over a range of SID collision energies. These plots are typically referred to as energy-resolved mass spectrometry (ERMS) plots. From the SID-ERMS plot generated for streptavidin (Figure 3A), not only is it evident that the streptavidin tetramer does not fragment directly to four monomers, because monomer onset is accompanied by trimer onset, but it is clear that monomer intensity increases as the dimer intensity decreases, which suggests secondary cleavage of the monomer-monomer interface within the dimer at higher SID collision energies. Furthermore, the various charge states of the SID products were monitored over a range of collision energies to determine the pathway responsible for the

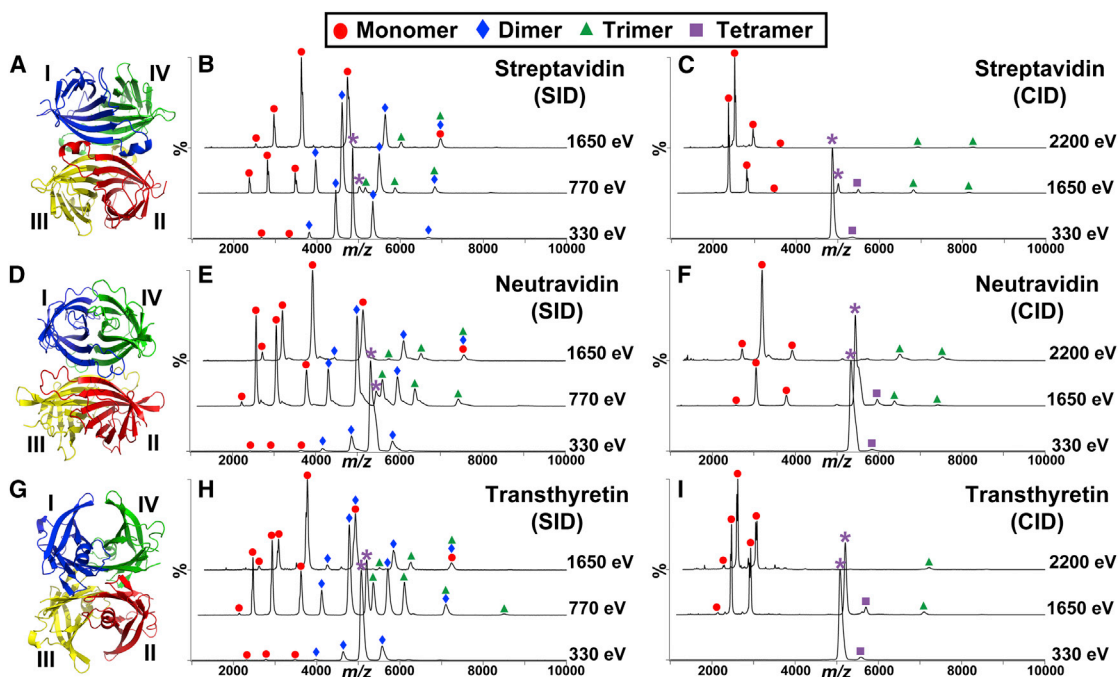


**Figure 1. Low-Energy SID Results in Dissociation Reflective of a Tetramer that Is a Dimer of Dimers, whereas CID Does Not**

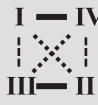
Nano-electrospray SID (middle panel) and CID (right panel) mass spectra of the charge-reduced +11 precursor of (B and C) SA, (E and F) neutravidin, and (H and I) TTR at three separate collision energies. All fragments are labeled based on their corresponding peaks detected in IM. The precursor ion in each spectrum is indicated by a purple asterisk. Crystal structures of (A) SA (PDB: 1SWB), (D) neutravidin (PDB: 1VYO), and (G) TTR (PDB: 1F41) are shown in the left panel. Subunits I, II, III, and IV are also shown in blue, green, yellow, and red, respectively.

increasing monomer intensity at higher SID collision energies. The results of this analysis for the streptavidin tetramer are shown in Figure 3B. From this plot, it is clear that the +3 and +4 monomer intensities increase with SID collision energy, while the +5 and +6 monomer (minor, but more unfolded) intensity is relatively constant. The relatively constant intensity of the trimer suggests that the dissociation of tetramer  $\rightarrow$  monomer + trimer is not a major contributor to the increasing monomer intensity. In contrast, the obvious decrease in the intensity of the +6 and +7 dimers suggests that higher SID collision energies results in dimer dissociation and symmetric charge partitioning between the ensuing monomer fragments (+6  $\rightarrow$  +3 & +3 and +7  $\rightarrow$  +3 & +4). SID-IM-SID experiments have also shown the direct conversion of dimer to monomer with symmetrical charge partitioning (unpublished data). These results further confirm that the relatively high abundance of low-charged monomers at high SID collision energies is primarily due to cleavage of the monomer-monomer interface within each initially formed dimer (I-IV and II-III).

Neutravidin is also a dimer of dimers (Repo et al., 2006), with secondary, tertiary, and quaternary structures almost identical to streptavidin (Laitinen et al., 2006). SID dissociation of the charge-reduced +11 neutravidin tetramer shows similar behavior to streptavidin, where dimer is produced at low energy (Figure 1E, 330 eV) and monomers are the primary products at higher SID collision energies (Figure 1E, 770 eV and 1650 eV). As was the case for streptavidin, dimer formation is the lowest energy pathway, consistent with cleavage of the lowest interface area, and monomer-trimer formation requires higher energy

input. The experimental CCS of the dimer obtained (Figure 2B) is consistent with cleavage of the smaller dimer-dimer interface (1388 Å<sup>2</sup>, Table 1) assuming no significant rearrangement of the dimer occurs in the time it spends between the SID and IM regions. A comparison of the amount of dimer observed for streptavidin and neutravidin at 330 eV (Figures 1B and 1E respectively) reveals that SID dissociation of the neutravidin tetramer produces less dimer, which may be attributed to the fact that the sum of the smaller dimer-dimer interfaces cleaved in the neutravidin tetramer (1388 Å<sup>2</sup>) is larger than that in the streptavidin tetramer (1176 Å<sup>2</sup>). This observation is further emphasized in the SID-ERMS plots for streptavidin and neutravidin (Figures 3A and 3C, respectively), where the maximum percentage of dimers observed for neutravidin (39%) is significantly lower than that seen for streptavidin (68%). In addition, the SID-ERMS plots generated for neutravidin and streptavidin not only show that SID dissociation of the neutravidin tetramer yields a greater fraction of trimer but that the increase in monomer observed at higher SID collision energies is accompanied by a decrease in the intensities of both dimer and trimer. As was the case with streptavidin, we utilized the relative abundances of the various charge states of SID products obtained with increasing collision energy (Figure 3D) to verify whether the increase in monomer intensity at higher SID collision energies was due to dimer and/or trimer dissociation. In contrast to streptavidin, an increasing amount of +4 and +5 dimer is observed at higher SID collision energies for neutravidin, which confirms that a portion of the increasing monomer intensity is due to dissociation of trimer (+7 trimer  $\rightarrow$  +3 monomer & +4 dimer

**Table 1. Interface Areas between Subunits and Dissociation Fragments**

	Individual interface area (Å <sup>2</sup> )		
	SA	NA	TTR
I ... II (III ... IV)	415	550	320
I --- III (II --- IV)	173	144	379
I — IV (II — III)	1551	1889	874
Fragments from tetramer dissociation	Interface area cleaved <sup>a</sup> (Å <sup>2</sup> )		
	1176	1388	1398
			
	2139	2583	1573
			
	3448	4066	2506
			
	3932	4878	2388
			
	4278	5166	3146
			

<sup>a</sup>Interface area cleaved is the sum of the interface areas involved in the cleavage of tetramer to produce fragments. For example, the interface area cleaved to produce transthyretin monomer and trimer is 874 Å<sup>2</sup> + 379 Å<sup>2</sup> + 320 Å<sup>2</sup>. Note that in production of monomer and trimer, I, II, III, or IV can be dissociated from tetramer with the same amount of interface area cleaved (i.e. there are four equivalent pathways available).

and +8 trimer → +3 monomer & +5 dimer). However, as these were only minor changes, it is not the main source of monomers. Instead, the increase in monomer at higher SID collision energies is primarily due to dissociation of the +6 and +7 dimer (+6 → +3 & +3 and +7 → +3 & +4). Hence, like streptavidin, higher energy SID of the neutravidin tetramer results in secondary cleavage of the monomer-monomer interface (1889 Å<sup>2</sup>) within each I-IV/II-III dimer to produce monomers.

We subsequently extended our SID analysis to TTR, which is also a dimer of dimers (Blake et al., 1978). While PISA analysis (shown in Table 1) illustrated that the largest interface in TTR is also the I-IV and II-III interface (874 Å<sup>2</sup> each), the other two interfaces in the TTR tetramer (I-III and II-IV, 379 Å<sup>2</sup> each; I-II and III-IV, 320 Å<sup>2</sup> each) are more similar than observed for streptavidin and neutravidin. Again, as was the case for streptavidin and

neutravidin, SID dissociation of the charge-reduced +11 TTR tetramer yields primarily dimer and monomers at low and higher SID collision energies, respectively (Figure 1H). Figure 2C illustrates that the experimental CCS calculated for the dimers obtained from SID shows good correlation with the theoretical CCS for the dimers expected from cleavage of the lowest total interface area (1,398 Å<sup>2</sup>). An examination of the SID-ERMS plot generated for TTR (Figure 3E) reveals that SID dissociation of TTR yields the lowest percentage of dimer (34%) and the highest percentage of trimer (19%) among the three homotetramers studied. We propose that this is due to the stronger contacts that exist across the dimer-dimer interface in TTR and the relatively similar total interface area needed to produce dimer (1398 Å<sup>2</sup>) versus monomer/trimer (1573 Å<sup>2</sup>). Even with the higher percentage of trimer observed for TTR, an analysis of the relative abundances of the various charge states of SID products obtained with increasing collision energy (Figure 3F) reveals that the major contributing factor to the increased monomer intensity observed at higher SID collision energies is the dissociation of the +6 and +7 dimers, which correlates with cleavage of the monomer-monomer interface within each dimer (I-IV and II-III).

#### Collision-Induced Dissociation of Homotetramers with D<sub>2</sub> Symmetry

As mentioned previously, CID is the most popular dissociation method available in commercial mass spectrometers. Consequently, we dissociated the three homotetramers over a range of collision energies to determine whether we could gain any information on the assembly of these homotetramers. From the CID spectra shown in Figures 1C, 1F, and 1I for streptavidin, neutravidin, and TTR, respectively, it is clear that the lab-frame energy required to dissociate the homotetramers via CID is much higher than that needed in SID. This is not surprising as SID is known to be a higher energy deposition process due to the more massive surface target (Blackwell et al., 2011; Zhou and Wysocki, 2014). CID of the homotetramer primarily yields highly charged monomer and its complementary low-charged trimer, even at the highest possible voltage difference within the instrument, e.g. CID collision energy (2200 eV) for the +11 tetramer. It should be noted that the contrasting intensities observed for monomer and trimer are typically seen in quadrupole time-of-flight (Q-TOF) instruments, and reflect in part the differing transmission and detection efficiencies of the fragments. The high charge on the monomer is consistent with an unfolded monomer plus a trimer rather than direct production of four monomers. Moreover, the CID-ERMS plots for streptavidin, neutravidin, and TTR (Figures S2A–S2C) offer limited insight into the assembly of the tetramers because these plots not only show no significant dimer present but also increasing intensities of monomer and trimer with increasing CID collision energy.

While the CID dissociation pathway is not consistent with the D<sub>2</sub> homotetramer assembly pathway, we analyzed the CID-ERMS plots obtained for streptavidin, neutravidin, and TTR to ascertain whether there was any additional information we could learn from the CID dissociation pathway. We observed a lower energy onset of monomer ejection for streptavidin (Figure S2A) compared with its homologue neutravidin (Figure S2B). This result matches well with the smaller trimer-monomer interface of streptavidin (shown in Table 1) and agrees with results from

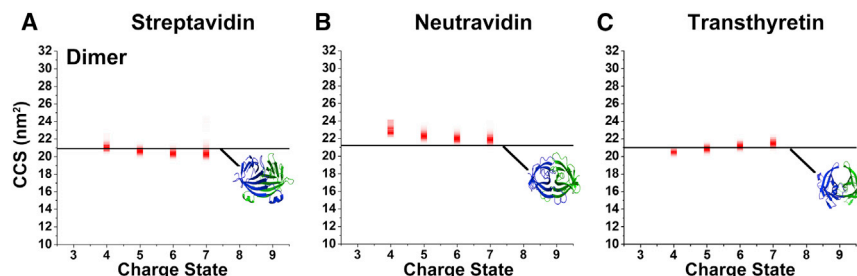


**Figure 2. Dimers Produced from SID Dissociation Have C<sub>2</sub> Symmetry**

Plots showing that the CCS of the dimer fragments produced from SID of the +11 precursor of (A) streptavidin (B) neutravidin, and (C) TTR correlate well with the expected CCS of C<sub>2</sub> dimers as calculated from the clipped structures, assuming no rearrangement prior to IM. It should be noted that the CCS of the products were similar over all the collision energies sampled for all SID experiments.

stability studies on thermally induced unfolding of neutravidin and streptavidin in the presence of high concentrations of guanidinium hydrochloride, which demonstrated that the midpoint denaturation temperature ( $T_m$ ) of neutravidin was 10°C higher than that of streptavidin (González et al., 1999). The proposed model for CID of a protein complex is described as the continuous unfolding of a monomer and charge migration until the interaction between the monomer and (n - 1)-mer are disrupted (Benesch et al., 2006). Hence, CID may provide information related to the ease of monomer unfolding and its interaction with its neighboring subunits, as was the case with streptavidin and neutravidin. However, the products observed in CID suggest that it is unable to give direct information on the relative strengths of the dimer-dimer interfaces in the tetramer, due to the unfolding behavior typically associated with CID and the lack of significant dimer products.

### Characterizing Effect of Ligand Binding

The increase in thermal stability of protein complexes upon ligand binding is due to the effect of binding on the unfolding equilibrium (Celej et al., 2003). Consequently, in this part of the study, we utilized SID to determine the effects that ligand binding has on both the stability and unfolding of the homotetramer. We first added biotin to both streptavidin and neutravidin and each +11 tetramer with four biotin molecules was dissociated via SID over a range of collision energies. The calculated masses of streptavidin and neutravidin show an increase equivalent to four biotin molecules, for both holo-streptavidin and holo-neutravidin tetramers (see Table S1). The low-energy (330 eV) SID spectra for the streptavidin and neutravidin holo-tetramer are shown in Figures 4A and 4C, respectively. SID of holo-streptavidin and holo-neutravidin tetramers yields a mixture of dimers with a range of 0–2 biotin molecules bound (it should be noted that the breadth of the peaks in Figure 4A is compromised by the fact that streptavidin also has variable N-terminal methionine inclusions). To determine whether SID could give any information on the relationship between stability and unfolding, the experimental CCS of the +11 tetramer (both apo and holo forms) following 330 eV surface collision were calculated using drift times obtained from SID-IM-MS experiments and compared. The results of this analysis are shown in Figures 4B and 4D for streptavidin and neutravidin, respectively, with apo shown on the left and holo on the right. The CCS plots for the SID of the apo forms of streptavidin and neutravidin show both folded and unfolded tetramer, whereas similar plots for the SID of holo-streptavidin and holo-neutravidin only show the presence of folded tetramer. These results illustrate that binding of biotin

leads to the stabilization of the native conformation of streptavidin and neutravidin, changing the energy required for unfolding in tetramer dissociation.

Next, we added thyroxine ( $T_4$ ) to TTR and dissociated the +11 tetramer over a range of SID collision energies. The low-energy SID spectrum of TTR with two  $T_4$  reveals a triplet of peaks for the TTR tetramer corresponding to zero, one, and two  $T_4$  molecules bound (Figure 4E). In addition, the calculated masses of the dimers produced from SID dissociation of apo and holo-TTR tetramers are 27,803 Da and 27,759 Da, respectively, which is close to the theoretical mass of 27,555 Da. Considering that the mass of  $T_4$  is 777 Da, the extra mass observed for the dimers is too low to be explained by retention of  $T_4$  by dimers from holo-TTR tetramer and is likely due to variable salt and solvent adducts as is typical in native mass spectrometry. As was the case for streptavidin and neutravidin, the effect of ligand binding on the stability and unfolding of the tetramer was also determined by comparing the CCS of both apo- and holo-TTR tetramer after activation via SID (Figure 4F). From the CCS plots obtained, it is evident that binding of two  $T_4$  results in only the folded TTR tetramer being present. We also discovered that the binding of only one  $T_4$  molecule leads to a lower amount of unfolded TTR tetramer relative to that seen for apo-TTR (results not shown), which suggests that the effect of stabilization of the native TTR tetramer is greater when both  $T_4$  binding sites are occupied.

To determine whether ligand binding has an effect on the interaction between subunits, we compared the relative intensities of fragments obtained from SID dissociation of holo and apo forms of the homotetramers over a range of similar collision energies (Figure S3). The comparison of the relative intensities of fragments obtained from SID dissociation of apo versus holo forms of streptavidin and neutravidin (Figures S3A and S3B, respectively) reveal that the binding of biotin results in a decrease of undissociated tetramer by less than 10% at energies where complete biotin loss has not yet occurred. This suggests that the binding of biotin leads to slightly more dissociation of holo-streptavidin and neutravidin tetramers. In contrast, the results for TTR (Figure S3C) reveal that binding of  $T_4$  to TTR results in an increase of undissociated tetramer by as much as 15%, accompanied by a decrease in the relative abundance of monomer and dimer fragments. This suggests that binding of  $T_4$  to the TTR tetramer results in the tetramer being more resistant to dissociation. Moreover, because the two  $T_4$  binding sites are located in a channel that runs through the dimer-dimer interface of the TTR tetramer (Wojtczak et al., 1996), the absence of  $T_4$  in the dimers is further evidence that SID results in cleavage of the

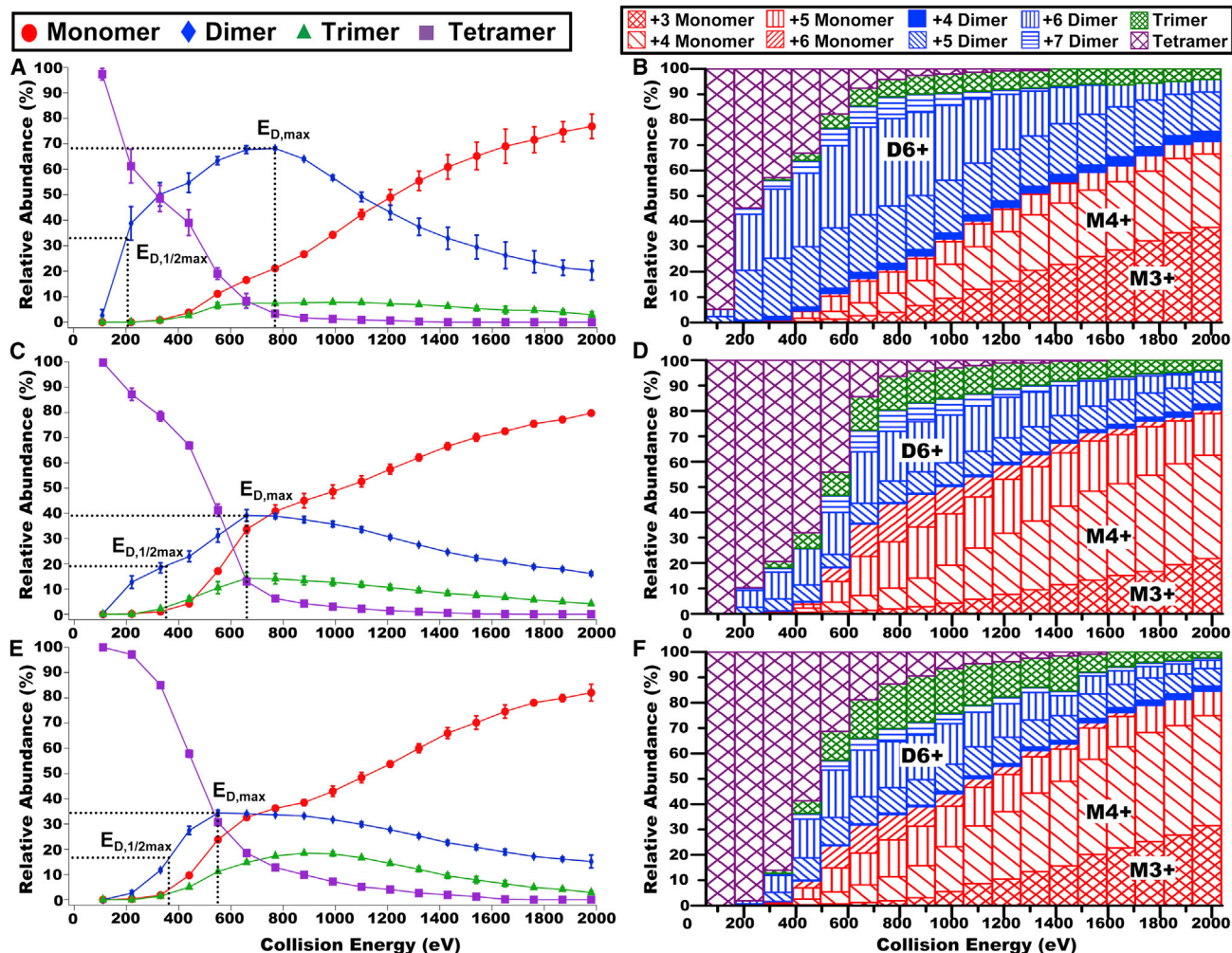


**Figure 3. SID Dissociation Pathway Occurs via Tetramer → Dimer → Monomer**

Energy-resolved plots showing the relative abundance of SID fragments produced from the charge-reduced +11 precursor of (A) streptavidin, (C) neutravidin, and (E) TTR. The SID collision energy where the maximum relative intensity of dimer occurs is labeled as  $E_{D,max}$  and the SID collision energy where half the maximum amount of dimer occurs is labeled as  $E_{D,1/2max}$ . The errors bars represent the SD of three independent measurements. Plots showing the relative abundance of the various charged SID fragments produced from the charge-reduced +11 precursor of (B) streptavidin, (D) neutravidin, and (F) TTR, as a function of collision energy are also shown.

lowest total interface area ( $1398 \text{ \AA}^2$ ) to produce I-IV and II-III dimers.

## DISCUSSION

Our results reveal that SID dissociation of a  $D_2$  homotetramer initially results in cleavage of the smaller dimer-dimer interfaces yielding  $C_2$  dimers, a structurally informative pathway that is not seen by the common CID activation method. SID dissociation at higher energies results in primary cleavage to dimers and secondary cleavage of the larger monomer-monomer interface within the  $C_2$  dimer to produce monomers. Moreover, a semi-quantitative comparison between the SID collision energies required for cleavage of the dimer-dimer interface in streptavidin, neutravidin, and TTR tests the validity of the assumption that the interface strength is proportional to the interface area

calculated from crystal structures. Because the appearance of dimers from tetramers occurs over a range of SID collision energies, we first determined the collision energy at which dimer intensity maximizes (represented as  $E_{D,max}$  in Figures 3A, 3C, and 3E), and then compared that with the collision energy at which half the maximum amount of dimer occurs ( $E_{D,1/2max}$ ). The similar  $E_{D,1/2max}$  values determined for neutravidin (360 eV) and TTR (370 eV) agree well with the similar dimer-dimer interface areas calculated for neutravidin ( $1388 \text{ \AA}^2$ ) and TTR ( $1398 \text{ \AA}^2$ ). In addition, the lower  $E_{D,1/2max}$  value determined for streptavidin (210 eV) correlates well with the smaller dimer-dimer interface for streptavidin ( $1176 \text{ \AA}^2$ ). However, the ratio of  $E_{D,1/2max}$  for streptavidin/neutravidin (1:1.7) is lower than the ratio of their corresponding dimer-dimer interface areas (1:1.2), which suggests that the neutravidin interface is stronger than revealed by interface area alone. A PISA analysis of the crystal structures of the three

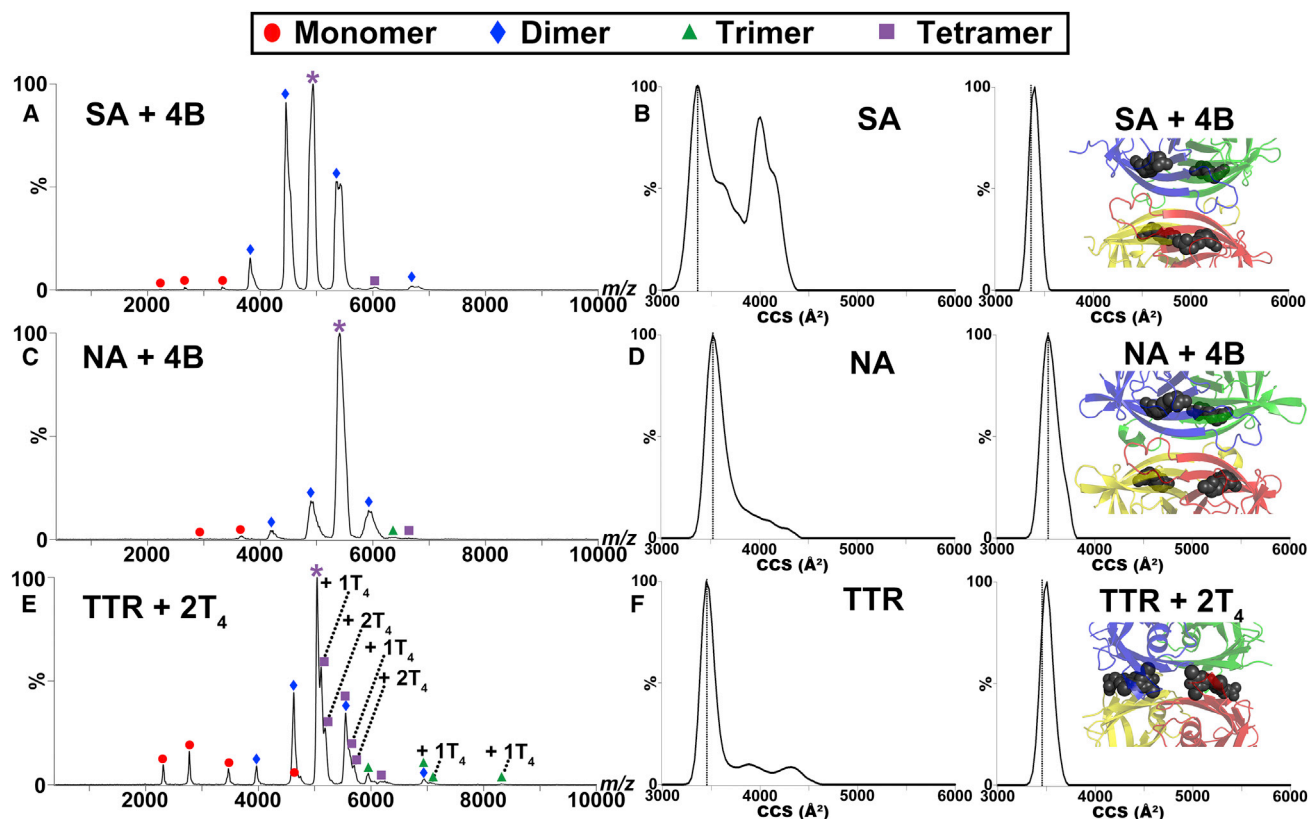


**Figure 4. Ligand Binding Results in Stabilization of Native Homotetramer**

Nano-electrospray SID mass spectra of the charge reduced +11 precursor of (A) streptavidin-biotin (C) neutravidin-biotin, and (E) TTR- $T_4$  complexes at a collision energy of 330 eV. TTR- $T_4$  tetrameric complex shows 1:1 (complex/ligand) and 1:2 stoichiometry (complex/ligand), whereas streptavidin-biotin and neutravidin-biotin tetrameric complexes show 1:4 stoichiometry. The precursor ion in each spectrum is indicated by a purple asterisk. Zoomed-in regions of the binding pockets of streptavidin-biotin (PDB: 3RY2), neutravidin-biotin (PDB: 1AVD), and TTR- $T_4$  (PDB: 2ROX) complexes are shown in the inset of the right panel. The ligand is shown as gray spheres. Subunits I, II, III, and IV are also shown in blue, green, yellow, and red, respectively. CCS plots showing apo- (left) versus holo- (right) forms of (B) streptavidin, (D) neutravidin, and (F) TTR at a SID collision energy of 330 eV are also shown. The native forms of the homotetramers (based on crystal structure) are indicated by the dotted lines.

homotetramers reveals that the number of possible H bonds formed at the dimer-dimer interface of neutravidin is equal to that of transthyretin but is 2.5 times that of streptavidin. (None of the complexes have salt bridges at the dimer-dimer interfaces, otherwise those would have also been considered.) This suggests that the energy required to break the dimer-dimer interface is not only related to the total interface area but also the number of interactions at the interface with the number of H bonds playing a greater role than the total relative interface area. Together, the above results show that by monitoring the SID products as a function of increasing collision energy, we are able to gain a fundamental mechanistic insight into the assembly of homotetramers because the SID dissociation pathway ( $D_2$  tetramer  $\rightarrow$   $C_2$  dimer  $\rightarrow$  monomer) observed for streptavidin, neutravidin, and TTR is simply the reverse of their assembly pathway. In addition, the SID collision energies associated with the appearance of dimers may be used as a means of characterizing different dimer-dimer interface areas and H-bonding sites that exist within  $D_2$  homotetramers.

The flexibility induced by  $D_2$  symmetry of homotetramers is believed to play a critical role in their biological function and

thus has direct implications in understanding structure-function relationships (Schulze et al., 2013; Spyralis et al., 2011). Furthermore, protein flexibility allows increased affinity to be achieved between a drug and its target by having a direct effect on the location of binding sites, binding orientation, and binding kinetics (Teague, 2003). While most structure-based drug design and molecular modeling studies are limited to the use of static structures (Cozzini et al., 2008), IM-MS can be used to study flexible biomolecules. By coupling SID with IM-MS, we observed unfolding of all three apo-tetramers upon SID activation, thereby indicating the presence of flexible regions within each tetramer. Ligand binding results in a decrease in conformational flexibility of the tetramers, which correlates to the folded state of the holo-tetramer being present (Figure 4). This decrease in flexibility also had an effect on the dissociation behavior, with SID of biotin-bound streptavidin and neutravidin tetramers yielding less than 10% lower intensities of undissociated holo-tetramer and a higher fraction of dimer compared with apo-tetramer. The binding of biotin has been previously shown to occur in a noncooperative fashion leading to four individual ligand binding sites with most of the protein-biotin interactions occurring within each

monomer (Deng et al., 2013; Hendrickson et al., 1989). Therefore, we hypothesize that the lower number of active degrees of freedom for the more rigid holo-tetramer may result in a higher proportion of the internal energy contributing to the dissociation of tetramer to dimer, whereas the internal energy of the more flexible apo-tetramer is shared between intra-complex monomer unfolding and dissociation of the tetramer to dimer.

Although binding of  $T_4$  to TTR also results in decreased flexibility, the SID dissociation behavior observed for holo-TTR is quite different to that seen for streptavidin and neutravidin with intact TTR tetramer intensities approximately 15% higher for holo- versus apo-TTR. These differences may be due to the different locations of the biotin-binding pockets of streptavidin and neutravidin and the  $T_4$  binding sites in TTR (see crystal structures in Figure 4). The biotin-binding site in both streptavidin and neutravidin is a pocket located at the end of the  $\beta$ -barrel of each monomer (Celej et al., 2004) and previous studies have shown that the biotin in one monomer only interacts with a single residue (Trp 120 in streptavidin and Trp 110 in avidin) in an adjacent monomer through the dimer-dimer interface (Sano and Cantor, 1995). In contrast, not only are the two  $T_4$  binding sites located at the dimer-dimer interface of the TTR tetramer but  $T_4$  binding results in formation of interactions between  $T_4$  and several residues present in the binding pockets. Therefore,  $T_4$  binding results in stabilization of the dimer-dimer interface which correlates to a larger amount of undissociated holo-tetramer than seen for the apo-tetramer at similar SID collision energies. This work suggests that SID-IM may be a useful tool for studying the effect of ligand binding by monitoring changes to the CCS and dissociation behavior of the protein complex.

## SIGNIFICANCE

Previous studies highlight that analysis of the interfaces within oligomers is critical to gaining insight into their assembly pathways (Perica et al., 2012) and that the solution disassembly pathway mimics the assembly pathway (Levy et al., 2008). While several strategies exist through which the dissociation patterns of homomers can be studied by mass spectrometry, they usually require multiple steps that involve solution perturbation and subsequent gas-phase dissociation and detection. Here, we employ direct surface-induced dissociation (SID) to predict the self-assembly of three  $D_2$  homotetramers and demonstrate that the SID dissociation pathway ( $D_2$  tetramer  $\rightarrow$   $C_2$  dimer  $\rightarrow$   $C_1$  monomer) is simply the reverse of the assembly pathway. Moreover, we illustrate that the SID collision energy associated with the  $D_2$  tetramer  $\rightarrow$   $C_2$  dimer transition shows good correlation with the dimer-dimer interface area and the intersubunit H-bonding interactions, and thus has potential to be used as an indicator of the relative strength of subunit interfaces. In addition, by monitoring the ligand-mediated changes to the CCS and relative abundance of undissociated tetramer utilizing SID-MS and ion mobility, we determined that ligand binding leads to reduced conformational flexibility. However, this does not always translate to increased stability of the tetramer because the dissociation of the complex is highly dependent on the location of the

binding site and the binding interactions, with increased propensity for dissociation possible if ligand increases intra-monomer rigidity and reduced propensity for dissociation possible if ligand involves direct bonding at a relevant interface. Current work in progress extends the approach described here to complexes with a variety of sizes, symmetries, and interface types.

## EXPERIMENTAL PROCEDURES

### Protein Preparation

TTR was purchased from Sigma-Aldrich, streptavidin and neutravidin from Thermo Scientific Pierce Biotechnology. Protein samples were diluted to 10  $\mu$ M and buffer exchanged into 100 mM ammonium acetate (pH 7.0) with 6-kDa cut-off size exclusion chromatography spin columns (Bio-Rad). A solution of 100 mM triethylammonium acetate (TEAA) was added to the protein samples in a 1:4 (TEAA/ammonium acetate) ratio to produce charge-reduced protein. TEAA and ammonium acetate were purchased from Sigma-Aldrich.

### Nanoelectrospray Ionization Mass Spectrometry Analysis

Nanoelectrospray ionization mass spectrometry (ESI MS) analysis was conducted by utilizing a modified quadrupole ion mobility time-of-flight (Q-IM-TOF) instrument (Synapt G2-S, Waters) with a customized SID device installed before the IM chamber (SID-IM) as previously described (Zhou et al., 2012). The direct current (DC) voltages on the lenses of our customized SID device are tuned differently depending on the experiments being conducted. In MS and CID experiments, similar voltages are applied to all the lenses in our customized SID device to allow for the transmission of ions without undergoing any surface collisions. The acceleration voltage in CID is defined by the Trap CE setting on the tune page in the instrument software and it is the potential difference between the DC offsets of the quadrupole and the trap traveling wave ion guide that acts as the collision cell in these experiments. In SID experiments, the voltages on the front deflector lenses are tuned to steer the ions onto the surface for collision and the rear deflector lenses are tuned to collect and steer the products to downstream optics. The acceleration voltage in SID is defined by the potential difference between the DC offset of the trap traveling wave ion guide and the surface, and can be adjusted using the Trap bias setting on the tune page in the instrument software. The collision energy, which is used as a means of comparing the relative strengths of the interfaces in this study, is calculated by multiplying the acceleration voltage by the charge state of the precursor. All experiments were conducted using a capillary voltage of 1.0–1.2 kV, cone voltage of 20 V, 2.4 mbar gas pressure in the IM cell, a gas flow rate of 120 ml/min into the helium cell, and a TOF analyzer pressure of  $\sim 6 \times 10^{-7}$  mbar. Wave conditions in the IM cell were as follows: wave velocity, 300 m/s; wave height, 20 V.

### IM Experiments

CCS calibration curves were generated following a published protocol (Bush et al., 2010) using four protein complexes as standards: transthyretin, avidin, concanavalin A, and serum amyloid P. The IM wave conditions chosen (wave velocity, 300 m/s; wave height, 20 V) yielded an  $R^2$  value of 0.998 for the calibration plot. Voltages in the instrument were tuned to ensure that activation between ion optics was minimized without compromising the transmission of ions.

### Theoretical CCS Calculation

Crystal structures of TTR (PDB: 1F41), streptavidin (PDB: 1SWB), and neutravidin (PDB: 1VYO) were obtained from the Protein Data Bank. Using Pymol, the crystal structures for fragments were obtained by removing the subunits not present. Hydrogen atoms were then added to the crystal structures using the BABEL software and the theoretical CCS values of the native complex were calculated using the Projection Approximation (PA) model (Mack, 1925) implemented in the open source software MOBCAL. The CCS values obtained were corrected as previously described (Hall et al., 2012) because the PA model typically underestimates CCS by approximately 14% (Shvartsburg

and Jarrold, 1996). The MOBCAL calculations were performed on the High Performance Computing servers at Ohio State University.

### SUPPLEMENTAL INFORMATION

Supplemental Information includes one table and three figures and can be found with this article online at <http://dx.doi.org/10.1016/j.chembiol.2015.03.019>.

### AUTHOR CONTRIBUTIONS

R.S.Q. and J.Y. performed the experiments and analyzed the data. R.S.Q. and J.Y. designed the figures and tables. R.S.Q. wrote the manuscript with input from J.Y. and V.H.W.

### ACKNOWLEDGMENTS

We are grateful for financial support from the National Science Foundation (NSF DBI 0923551 to V.H.W.). An allocation of computer time from the Ohio Supercomputing Center at Ohio State University is also gratefully acknowledged.

Received: November 30, 2014

Revised: March 23, 2015

Accepted: March 26, 2015

Published: April 30, 2015

### REFERENCES

- Benesch, J.L.P., Aquilina, J.A., Ruotolo, B.T., Sobott, F., and Robinson, C.V. (2006). Tandem mass spectrometry reveals the quaternary organization of macromolecular assemblies. *Chem. Biol.* *13*, 597–605.
- Blackwell, A.E., Dodds, E.D., Bandarian, V., and Wysocki, V.H. (2011). Revealing the quaternary structure of a heterogeneous noncovalent protein complex through surface-induced dissociation. *Anal. Chem.* *83*, 2862–2865.
- Blake, C.C.F., Geisow, M.J., Oatley, S.J., Rérat, B., and Rérat, C. (1978). Structure of prealbumin: secondary, tertiary and quaternary interactions determined by Fourier refinement at 1.8 Å. *J. Mol. Biol.* *121*, 339–356.
- Bush, M.F., Hall, Z., Giles, K., Hoyes, J., Robinson, C.V., and Ruotolo, B.T. (2010). Collision cross sections of proteins and their complexes: a calibration framework and database for gas-phase structural biology. *Anal. Chem.* *82*, 9557–9565.
- Celej, M.S., Montich, G.G., and Fidelio, G.D. (2003). Protein stability induced by ligand binding correlates with changes in protein flexibility. *Protein Sci.* *12*, 1496–1506.
- Celej, M.S., Montich, G.G., and Fidelio, G.D. (2004). Conformational flexibility of avidin: the influence of biotin binding. *Biochem. Biophysical Res. Commun.* *325*, 922–927.
- Chen, J., Sawyer, N., and Regan, L. (2013). Protein-protein interactions: general trends in the relationship between binding affinity and interfacial buried surface area. *Protein Sci.* *22*, 510–515.
- Cozzini, P., Kellogg, G.E., Spyraakis, F., Abraham, D.J., Costantino, G., Emerson, A., Fanelli, F., Gohlke, H., Kuhn, L.A., Morris, G.M., et al. (2008). Target flexibility: an emerging consideration in drug discovery and design. *J. Med. Chem.* *51*, 6237–6255.
- Deng, L., Kitova, E., and Klassen, J. (2013). Dissociation kinetics of the streptavidin–biotin interaction measured using direct electrospray ionization mass spectrometry analysis. *J. Am. Soc. Mass Spectrom.* *24*, 49–56.
- González, M.N., Argaraña, C.E., and Fidelio, G.D. (1999). Extremely high thermal stability of streptavidin and avidin upon biotin binding. *Biomol. Eng.* *16*, 67–72.
- Goodsell, D.S., and Olson, A.J. (2000). Structural symmetry and protein function. *Annu. Rev. Biophys. Biomol. Struct.* *29*, 105–153.
- Green, N.M. (1990). [5] Avidin and streptavidin. In *Methods Enzymol.*, Vol. 184, W. Meir and A.B. Edward, eds. (Academic Press), pp. 51–67.
- Gupta, R., Hamdan, S.M., Dixon, N.E., Sheil, M.M., and Beck, J.L. (2004). Application of electrospray ionization mass spectrometry to study the hydrophobic interaction between the  $\epsilon$  and  $\theta$  subunits of DNA polymerase III. *Protein Sci.* *13*, 2878–2887.
- Hall, Z., Politis, A., Bush, M.F., Smith, L.J., and Robinson, C.V. (2012). Charge-state dependent compaction and dissociation of protein complexes: insights from ion mobility and molecular dynamics. *J. Am. Chem. Soc.* *134*, 3429–3438.
- Hendrickson, W.A., Pähler, A., Smith, J.L., Satow, Y., Merritt, E.A., and Phizackerley, R.P. (1989). Crystal structure of core streptavidin determined from multiwavelength anomalous diffraction of synchrotron radiation. *Proc. Natl. Acad. Sci. USA* *86*, 2190–2194.
- Hernandez, H., and Robinson, C.V. (2007). Determining the stoichiometry and interactions of macromolecular assemblies from mass spectrometry. *Nat. Protoc.* *2*, 715–726.
- Hyung, S.-J., Robinson, C.V., and Ruotolo, B.T. (2009). Gas-phase unfolding and disassembly reveals stability differences in ligand-bound multiprotein complexes. *Chem. Biol.* *16*, 382–390.
- Jones, C.M., Beardsley, R.L., Galhena, A.S., Dagan, S., Cheng, G., and Wysocki, V.H. (2006). Symmetrical gas-phase dissociation of noncovalent protein complexes via surface collisions. *J. Am. Chem. Soc.* *128*, 15044–15045.
- Kapur, A., Beck, J.L., Brown, S.E., Dixon, N.E., and Sheil, M.M. (2002). Use of electrospray ionization mass spectrometry to study binding interactions between a replication terminator protein and DNA. *Protein Sci.* *11*, 147–157.
- Kelly, J.W. (1997). Amyloid fibril formation and protein misassembly: a structural quest for insights into amyloid and prion diseases. *Structure* *5*, 595–600.
- Kershaw, N.J., McNaughton, H.J., Hewitson, K.S., Hernández, H., Griffin, J., Hughes, C., Greaves, P., Barton, B., Robinson, C.V., and Schofield, C.J. (2002). ORF6 from the clavulanic acid gene cluster of *Streptomyces clavuligerus* has ornithine acetyltransferase activity. *Eur. J. Biochem.* *269*, 2052–2059.
- Krissinel, E., and Henrick, K. (2007). Inference of macromolecular assemblies from crystalline state. *J. Mol. Biol.* *372*, 774–797, 'Protein interfaces, surfaces and assemblies' service PISA at the European Bioinformatics Institute. [http://www.ebi.ac.uk/pdbe/prot\\_int/pistart.html](http://www.ebi.ac.uk/pdbe/prot_int/pistart.html).
- Laitinen, O.H., Hytönen, V.P., Nordlund, H.R., and Kulomaa, M.S. (2006). Genetically engineered avidins and streptavidins. *Cell Mol Life Sci* *63*, 2992–3017.
- Levy, E.D., Pereira-Leal, J.B., Chothia, C., and Teichmann, S.A. (2006). 3D complex: a structural classification of protein complexes. *PLoS Comput. Biol.* *2*, e155.
- Levy, E.D., Erba, E.B., Robinson, C.V., and Teichmann, S.A. (2008). Assembly reflects evolution of protein complexes. *Nature* *453*, 1262–1265.
- Light-Wahl, K.J., Schwartz, B.L., and Smith, R.D. (1994). Observation of the noncovalent quaternary associations of proteins by electrospray ionization mass spectrometry. *J. Am. Chem. Soc.* *116*, 5271–5278.
- Luque, I., Leavitt, S.A., and Freire, E. (2002). The linkage between protein folding and functional cooperativity: two sides of the same coin? *Annu. Rev. Biophys. Biomol. Struct.* *31*, 235–256.
- Mack, E. (1925). Average cross-sectional areas of molecules by gaseous diffusion methods. *J. Am. Chem. Soc.* *47*, 2468–2482.
- Marsh, J.A., and Teichmann, S.A. (2014). Structure, dynamics, assembly, and evolution of protein complexes. *Annu. Rev. Biochem.* <http://dx.doi.org/10.1146/annurev-biochem-060614-034142>.
- Nencetti, S., and Orlandini, E. (2012). TTR fibril formation inhibitors: is there a SAR? *Curr. Med. Chem.* *19*, 2356–2379.
- Ng, D.P., Poulsen, B.E., and Deber, C.M. (2012). Membrane protein misassembly in disease. *Biochim. Biophys. Acta* *1818*, 1115–1122.
- Okorokov, A.L., Sherman, M.B., Plisson, C., Grinkevich, V., Sigmundsson, K., Selivanova, G., Milner, J., and Orlova, E.V. (2006). The structure of p53 tumour suppressor protein reveals the basis for its functional plasticity. *EMBO J.* *25*, 5191–5200.
- Perica, T., Chothia, C., and Teichmann, S.A. (2012). Evolution of oligomeric state through geometric coupling of protein interfaces. *Proc. Natl. Acad. Sci. USA* *109*, 8127–8132.

- Quintyn, R., Zhou, M., Dagan, S., Finke, J., and Wysocki, V. (2013). Ligand binding and unfolding of tryptophan synthase revealed by ion mobility-tandem mass spectrometry employing collision and surface induced dissociation. *Int. J. Ion Mobil. Spec.* *16*, 133–143.
- Repo, S., Paldanius, T.A., Hytönen, V.P., Nyholm, T.K.M., Halling, K.K., Huuskonen, J., Pentikäinen, O.T., Rissanen, K., Slotte, J.P., Airene, T.T., et al. (2006). Binding properties of HABA-Type Azo derivatives to avidin and avidin-related protein 4. *Chem. Biol.* *13*, 1029–1039.
- Sano, T., and Cantor, C.R. (1995). Intersubunit contacts made by tryptophan 120 with biotin are essential for both strong biotin binding and biotin-induced tighter subunit association of streptavidin. *Proc. Natl. Acad. Sci. USA* *92*, 3180–3184.
- Schulze, B., Sijoka, A., and Whiteley, W. (2013). How does symmetry impact the flexibility of proteins? *Philos. Trans. A Math. Phys. Eng. Sci.* *372*, 20120041.
- Shen, H.-B., and Chou, K.-C. (2009). QuatIdent: a web server for identifying protein quaternary structural attribute by fusing functional domain and sequential evolution information. *J. Proteome Res.* *8*, 1577–1584.
- Shvartsburg, A.A., and Jarrold, M.F. (1996). An exact hard-spheres scattering model for the mobilities of polyatomic ions. *Chem. Phys. Lett.* *261*, 86–91.
- Spyrakakis, F., BidonChanal, A., Barril, X., and Luque, F.J. (2011). Protein flexibility and ligand recognition: challenges for molecular modeling. *Curr. Top. Med. Chem.* *11*, 192–210.
- Teague, S.J. (2003). Implications of protein flexibility for drug discovery. *Nat. Rev. Drug Discov.* *2*, 527–541.
- Villar, G., Wilber, A.W., Williamson, A.J., Thiara, P., Doye, J.P.K., Louis, A.A., Jochum, M.N., Lewis, A.C.F., and Levy, E.D. (2009). Self-assembly and evolution of homomeric protein complexes. *Phys. Rev. Lett.* *102*, 118106.
- Weber, P.C., Ohlendorf, D.H., Wendoloski, J.J., and Salemme, F.R. (1989). Structural origins of high-affinity biotin binding to streptavidin. *Science* *243*, 85–88.
- Wetzel, R. (1996). For protein misassembly, it's the "I" decade. *Cell* *86*, 699–702.
- Wojtczak, A., Cody, V., Luft, J.R., and Pangborn, W. (1996). Structures of human transthyretin complexed with thyroxine at 2.0 Å resolution and 3',5'-dinitro-N-acetyl-L-thyronine at 2.2 Å resolution. *Acta Crystallogr. D Biol. Crystallogr.* *52*, 758–765.
- Zhou, M., and Wysocki, V.H. (2014). Surface induced dissociation: dissecting noncovalent protein complexes in the gas phase. *Acc. Chem. Res.* *47*, 1010–1018.
- Zhou, M., Dagan, S., and Wysocki, V.H. (2012). Protein subunits released by surface collisions of noncovalent complexes: native-like compact structures revealed by ion mobility mass spectrometry. *Angew. Chem. Int. Ed. Engl.* *51*, 4336–4339.
- Zhou, M., Jones, C.M., and Wysocki, V.H. (2013). Dissecting the large noncovalent protein complex GroEL with surface-induced dissociation and ion mobility-mass spectrometry. *Anal. Chem.* *85*, 8262–8267.